applied optics

Dispersion characteristics of a suspended-core optical fiber infiltrated with water

Khoa Dinh Xuan,[1] Lanh Chu Van,[1] Van Cao Long,[2] Quang Ho Dinh,[1] Luu Van Xuan,[1] Marek Trippenbach,[3] and Ryszard Buczynski[3,4,*]

[1]Department of Physics, Vinh University, 182 Le Duan Street, Vinh City, Vietnam
[2]Institute of Physics, University of Zielona Góra, Prof. Szafrana 4a, 65-516 Zielona Góra, Poland
[3]Faculty of Physics, University of Warsaw, Pasteura 7, 02-093 Warsaw, Poland
[4]Department of Glass, Institute of Electronic Materials Technology, Wólczynska 133, 01-919 Warsaw, Poland
*Corresponding author: rbuczyns@igf.fuw.edu.pl

Received 31 October 2016; revised 28 December 2016; accepted 30 December 2016; posted 3 January 2017 (Doc. ID 278887); published 26 January 2017

In this paper we present a study on the dispersion characteristics in the suspended-core optical fibers made of borosilicate of NC21A glass infiltrated with water. Replacement of air with water results in dramatic improvement of the dispersion characteristics in the fibers, valuable in the process of supercontinuum generation. A near-zero flat dispersion can be achieved in the anomalous or normal dispersion range for various diameters of the core. ©2017 Optical Society of America

OCIS codes: (260.2030) Dispersion; (060.5295) Photonic crystal fibers; (160.2750) Glass and other amorphous materials; (240.3990) Micro-optical devices.

https://doi.org/10.1364/AO.56.001012

1. INTRODUCTION

Suspended-core fibers (SCFs) are a subclass of microstructured fibers [1,2]. They are composed of a small core suspended between, usually, three submicron-thin glass bridges. These fibers possess a unique property that a part of the mode field is located beyond the glass area, which makes it a perfect component for sensing gas and liquids with evanescent fields or surface-plasmon generation when an additional thin gold layer is deposited on the core side walls [3,4]. In principle, a hollow-core fiber has similar properties. However, in the case of suspended-core fibers, their transmission is not limited to a small range of wavelengths defined by a bandgap structured of photonic crystal. The SCFs guide in the full range of transmission of glass since in this case the guiding mechanism consists of the effective total internal reflection. The SCFs are widely used for pressure, temperature, and gas sensing [5,6]. Recently, SCFs were also studied in the context of application as a medium for chemical and biomedical sensors [7,8]. Note that the side walls of the core can be easily functionalized with various thin layers selectively sensitive for chemical compounds or biomolecules. Several applications for explosive detection and DNA identification have already been reported [9–11], as well as application for the excitation of whispering gallery mode resonances into a microsphere encapsulated into the one of air holes of the SCF [12].

SCFs are also attractive for nonlinear optics application due to the strong confinement of light in the small core [13]. Up to now, the most important applications are soliton self-frequency shift [14], third-harmonic generation [15], Raman wavelength shift [16], optical parametric oscillators, and last, but not least, supercontinuum generation [16,17].

In the case of nonlinear applications it is necessary to engineer the dispersion of the fiber. There are many studies addressing the dispersion engineering of SCFs [18–20], but mainly attention is focused on the optimization of the cross-section parameters of the fiber. Particularly, the influence of the number and thickness of the glass bridges, and the diameter of the core on the dispersion characteristics were investigated [21]. However, a range of parameter changes were limited to only a few modes and SCFs with high mode confinement were considered. Here we claim that extra degrees of freedom are available when we consider a change of glass type or infiltration of air holes with gasses or liquids.

The possibility of dispersion curve modification by filling the air holes with water in a hollow-core photonic crystal fiber (PCF) made of fused silica glass, and SC generation in those fibers, was previously demonstrated. Bozolan *et al.* have shown the first experimentally successful anomalous supercontinuum generation in 5 cm long hollow-core PCF filled with water. A spectrum in the range 600–1140 nm is achieved [22]. Bethge *et al.* reported two-octave broad high-power anomalous SC in 9.5 μm hollow core PCF filled with water using 40 fs pulses at a pump wavelength of 1.2 μm with a pulse energy of

7 μJ [23]. Modifications of dispersion characteristics of hollow-core PCFs filled with various liquids were presented by Karasawa [24].

Recently, a soliton-based SC generation in solid-core regular lattice PCF with selectively water-filled holes was reported [25]. A spectrum from 450 to 1000 nm was obtained with 50 fs pulses at wavelength of 804 nm.

In this paper we propose to optimize the dispersion characteristics of SCFs by infiltrating holes with water. For the SCF, we assume a structure with the core suspended over three bridges and borosilicate NC-21A glass as the fiber material. Our motivation was to study the influence of water since it is the most common solvent used for different organic components and biomolecules. Water can be further modified with bioluminescent particles used as a nonlinear medium to stimulate supercontinuum generation.

2. MODELING MODAL AND DISPERSION PROPERTIES OF SUSPENDED-CORE FIBER

For simulation we used a SCF with three air holes made of borosilicate glass labeled NC-21A (Fig. 1). This multi-component glass, synthesized in-house at the Institute of Electronic Materials Technology in Poland (ITME), has an oxide composition by weight of 55.0% SiO_2, 1.0% Al_2O_3, 26.0% B_2O_3, 3.0% Li_2O, 9.5% Na_2O, 5.5% K_2O, and 0.8% As_2O_3 [26]. This glass is well suited for the development of complex fiber structures with the stack and draw technology due to its very good rheological properties. It has been successfully used for the development of microstructured fibers with complex structures, such as photonic crystal fibers with elliptical holes in photonic cladding, nanoholes in the core of fibers, or with a double core [27–30]. The main physical properties of NC21A are as follows: refractive index $n_D = 1.533$, density $\rho = 2.50$ g/cm^3, coefficient of thermal expansion $\alpha = 82 \times 10^{-7}$ K^{-1} for the range of 20–300°C, glass transition temperature $T_g = 500$°C, and softening point DTM = 530°C. The transmission of NC-21A glass is limited to the range 380–2700 nm with a relatively high attenuation of 4 dB/m.

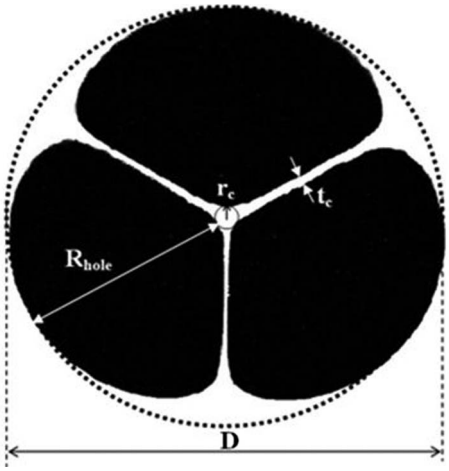

Fig. 1. Cross section of SCF of three bridges. White area denotes borosilicate glass; black area is air or water.

In the current design we consider the holes in the SCF to be infiltrated with air or with water. For modeling we use the commercial software Mode Solution by Lumerical based on the finite difference method [31]. This method is commonly used for calculations of the modal properties of photonic crystal fibers. The accuracy of the method strongly depends on the mesh resolution settings. We assume in our simulations a mesh resolution at the level $\lambda/10$. As a result, the calculation accuracy of the effective refractive index n_{eff} is 10^{-5}. A further increase of the mesh resolution does not increase the accuracy of calculation due to the accumulation of numerical errors; moreover, it dramatically increases calculation time [31]. The obtained accuracy of n_{eff} is satisfactory, since good agreement between model and experimental results are usually received [32].

$$n^2_{\text{NC21A}}(\lambda) = 1 + \frac{B_1\lambda^2}{\lambda^2 - C_1} + \frac{B_2\lambda^2}{\lambda^2 - C_2} + \frac{B_3\lambda^2}{\lambda^2 - C_3}, \quad (1)$$

where constant coefficients are given in Table 1.

The refractive index of water as a function of optical wavelength, temperature, and pressure is given by [33] and shown in Fig. 2:

$$\begin{aligned} n(\lambda, T, p) = &\sqrt{\frac{a_1}{\lambda^2 - \lambda_a^2} + a_2 + a_3\lambda^2 + a_4\lambda^4 + a_5\lambda^6} \\ &+ (b_1 + b_2\lambda^2 + b_3\lambda^4)(T - T_b) \\ &+ (b_4 + b_5\lambda^2 + b_6\lambda^4)(T - T_b)^2 \\ &+ (b_7 + b_8\lambda^2 + b_9\lambda^4)(T - T_b)^3, \end{aligned} \quad (2)$$

Table 1. Sellmeier Coefficients for Borosilicate Glass NC-21A [26]

Glass	NC-21A
B_1	0.64711
B_2	0.64711
B_3	98.02462
C_1 [μm^2]	0.09442
C_2 [μm^2]	0.09442
C_3 [μm^2]	112.597

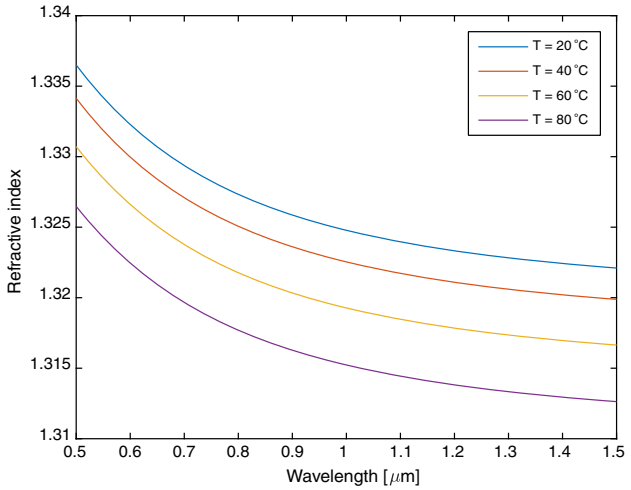

Fig. 2. Refractive index of water for different temperatures.

where $\lambda_a = 0.018085$, $a_1 = 5.743534 \times 10^{-3}$, $a_2 = 1.769238$, $a_3 = -2.797222 \times 10^{-2}$, $a_4 = 8.715348 \times 10^{-3}$, $a_5 = -1.413942 \times 10^{-3}$, $b_1 = -8.454823 \times 10^{-5}$, $b_2 = -2.787742 \times 10^{-5}$, $b_3 = 2.608176 \times 10^{-6}$, $b_4 = -2.050671 \times 10^{-6}$, $b_5 = 1.019989 \times 10^{-6}$, $b_6 = -2.611919 \times 10^{-6}$, $b_7 = 8.194989 \times 10^{-9}$, $b_8 = -8.107707 \times 10^{-9}$, $b_9 = 4.877274 \times 10^{-8}$, and $T_b = 19.993$°C.

For the preliminary stage of our simulations, we consider a real structure of the SCF made of boron-silicate glass, developed recently in ITME (Fig. 3). In modeling, we take into account all imperfections of the real structures. The effective parameters of the fiber are as summarized in Table 2.

The fiber considered here guides several modes in the visible range. The fundamental mode LP_{01} has a regular Gaussian-like shape and is localized at the cross section of the glass bridges. It is composed of two linearly polarized components. Higher-order modes correspond to LP_{11} and other higher-order modes (HOM). These properties are typical for SCFs. Geometrical losses (without taking into account material losses) of the fundamental mode LP_{01} are below 10^{-2} dB/m, while losses for HOMs are above 10 dB/m for the infrared range above 1000 nm. This attenuation is further increased if the SCF is infiltrated with water. Therefore, we can assume that this fiber is effectively single-mode in our case. An increase of temperature results in a small increase of refractive index contrast between the glass core and water in the fiber holes. As a result, the fundamental mode is better localized in the solid core and its effective mode area is slightly reduced. However, these changes are negligible with respect to plot resolution in Fig. 4.

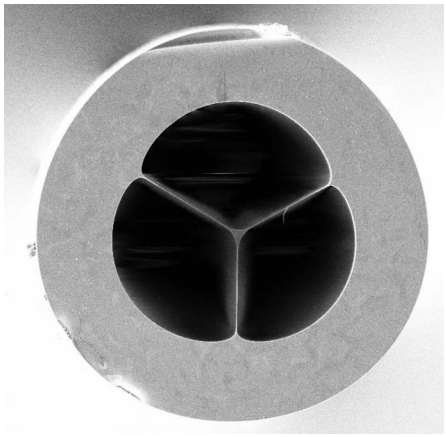

Fig. 3. SEM photo of SCF #1 made of borosilicate glass. Total diameter of air hole structure is 32.14 μm.

Table 2. Geometrical Parameters of Fabricated SCF Labeled #1 Made of Silicate Glass

No.	#1
Core diameter $2r_c$ [μm]	1.64
Thickness of glass bridges t_c [μm]	0.25
Radius of holes R_{hole} [μm]	15.23
Total diameter of air-hole structure D [μm]	32.14

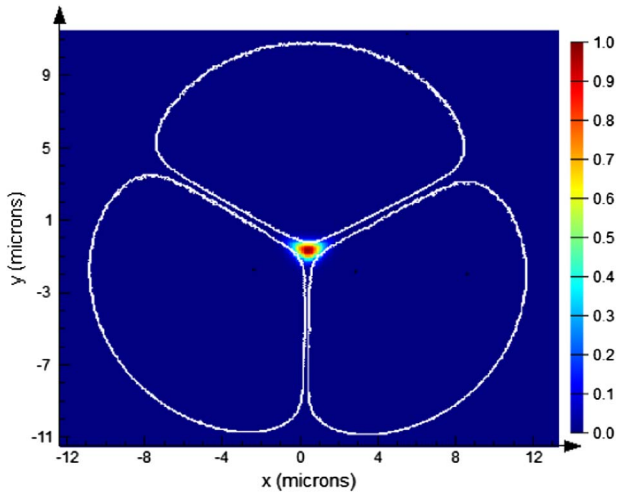

Fig. 4. Calculation of intensity distribution in the fundamental mode in SCF #1 for wavelength of 1064 nm and temperature 20°C.

We have calculated dispersion characteristics for the fundamental mode of the SCF with air holes and holes infiltrated with water at different temperatures of water: 20°C, 40°C, 60°C, and 80°C. Results are presented in Fig. 5. For the SCF infiltrated with air, we obtained typical characteristics for SCFs with relatively high anomalous dispersion and a zero dispersion wavelength (ZDW) below 800 nm.

We observe that when holes are infiltrated with water, the dispersion characteristics are more flat, and the value of dispersion is reduced by over 100 ps/nm/km. And, what is very important, the ZDW is shifted toward longer wavelengths to 984 nm.

Changing the temperature of the water results in further modification of the dispersion characteristics. When the temperature increases, the dispersion characteristics become more flat, the ZDW is shifted toward longer wavelengths, and all dispersion curvatures are shifted down toward normal dispersion.

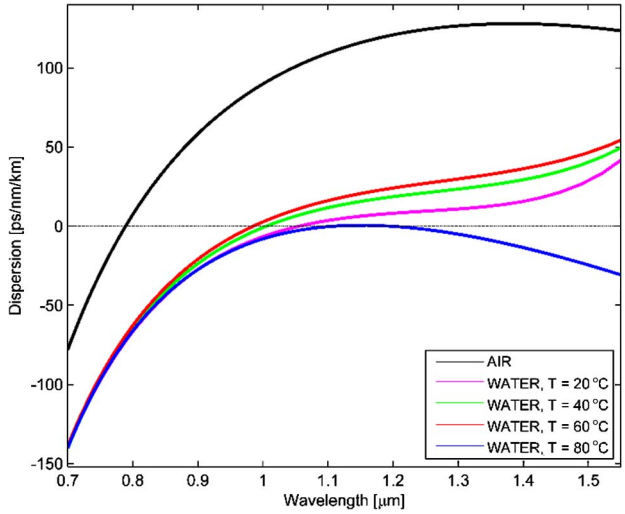

Fig. 5. Dispersion characteristics of SCF #1 infiltrated with air and water at different temperatures.

Table 3. Geometrical Parameters of Modeled SCF Made of Silicate Glass

Fiber	D (μm)	r_c (μm)	t_c (μm)	R_{hole} (μm)	Scale [%]
#2	19.28	0.5	0.15	9.14	60
#3	25.71	0.66	0.20	9.14	80
#1	32.14	0.82	0.25	15.23	100
#4	38.57	1.33	0.30	9.12	120
#5	44.99	1.55	0.35	9.14	140

3. MODIFICATION OF DISPERSION PROPERTIES FOR SUSPENDED-CORE FIBERS WITH VARIOUS SIZES

To verify the modification potential of dispersion characteristics in SCFs, we have performed a series of simulations for various sizes of SCFs. Having in mind the scalability of fiber drawing technology, we may assume that the total diameter and other parameters can be modified within a certain reasonable range. Hence for our simulations, to give a wider picture, we used several sets of parameters rescaled in comparison to those used for fabricated fiber #1. Our proposed values of parameters are presented in Table 3.

We have calculated the dispersion characteristics for all fibers infiltrated with air and water at different temperatures in the range 20°C–80°C (Figs. 6–9). To simplify discussion, we define a near-zero dispersion (NZD) band as an area where dispersion varies in the range between −100 to 100 ps/nm/km. These types of dispersion characteristics are highly demanded for effective supercontinuum generation, both coherent (normal dispersion) and soliton-fission-driven supercontinuum (anomalous dispersion).

Results of our investigations show that the total diameter of the air hole structure determines the offset of the dispersion characteristics with respect to the dispersion axis and the position of the first and second ZDW. The localization of the first ZDW is redshifted when the core diameter increases. For fiber #1 with the core diameter of 1 μm, ZDW is equal to 680 nm (Fig. 6), while for fiber #5 with the core diameter of 3.1 μm, ZDW achieves the value of 845 nm (Fig. 9). As a result, a simple rescaling of the SCF made of borosilicate glass does not allow the ZDW to shift to the proximity of 1064 nm. Moreover, a SCF with a core diameter larger than 1.8 μm with holes infiltrated with air cannot be treated as an effectively single-mode fiber and its application for supercontinuum generation is limited since higher-order modes are also excited when it is pumped.

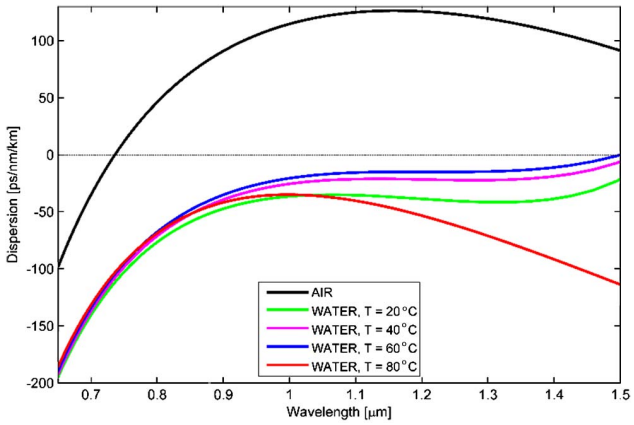

Fig. 7. Dispersion characteristics of SCF #3 infiltrated with air and water at different temperatures. Total diameter of air hole structure is $D = 25.7$ μm.

The localization of the second ZDW is also redshifted if the core dimeter increases. For fiber #1 with the core diameter of 1 μm, the second ZDW is 1358 nm (Fig. 6). When core diameter increases, the localization of the second ZDW shifts beyond 1500 nm and all fibers have anomalous dispersion in the range considered for visible to near-infrared supercontinuum generation. A larger diameter of the core usually results in more flat dispersion and the second ZDW is shifted toward a longer wavelength.

Unfortunately, none of the fibers considered here can be efficiently used for broadband supercontinuum generation, since the dispersion characteristics do not fit into NZD band in the near-infrared range.

Infiltration of air holes with water dramatically changes the dispersion characteristics of the considered SCFs. It always

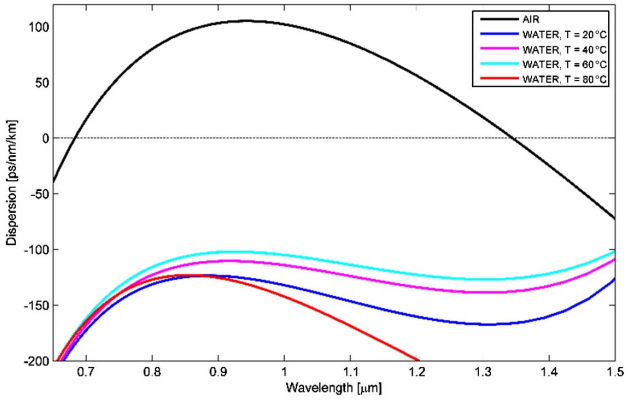

Fig. 6. Dispersion characteristics of SCF #2 infiltrated with air and water at different temperatures. Total diameter of air hole structure is $D = 19.3$ μm.

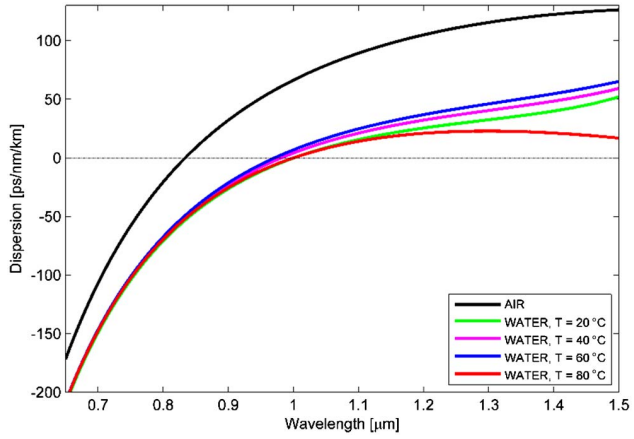

Fig. 8. Dispersion characteristics of SCF #4 infiltrated with air and water at different temperatures. Total diameter of air hole structure is $D = 38.6$ μm.

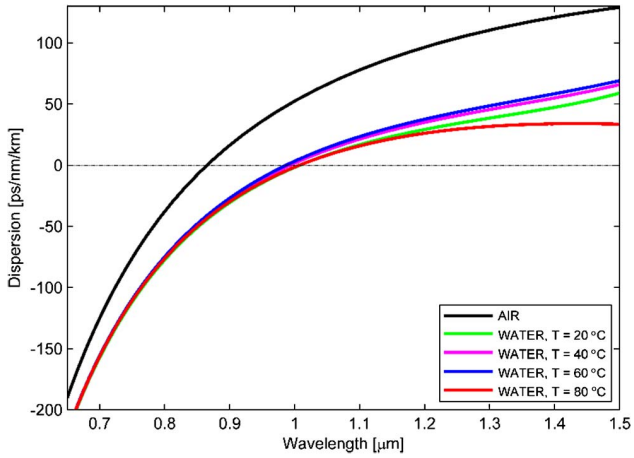

Fig. 9. Dispersion characteristics of SCF #5 infiltrated with air and water at different temperatures. Total diameter of air hole structure is $D = 44.9$ μm.

results in flattening dispersion characteristics with respect to SCFs with air. This phenomenon is well known in all-solid photonic crystal fibers [32]. It is a result of the reduction of contrast in fiber structure and the introduction of material with non-zero material dispersion instead of air. A localization of the first ZDW is shifted toward longer wavelengths with respect to air-infiltrated SCFs for the fibers with a core diameter larger than 1.52 μm (fibers #1, #4, #5). The ZDW is redshifted over 100 nm. For fiber #1, the ZDW achieves 984 nm, while for other fibers, #4 and #5, the ZDWs are 972 nm and 968 nm, respectively. Shifting the ZDW toward 1000 nm is extremely important if we consider use of the SCFs for supercontinuum generation with low-cost short-pulse microchip lasers. The fibers with small cores, #1 and #2, have normal dispersion in all considered near-infrared ranges. All these fibers are good candidates for the generation of a soliton-driven supercontinuum.

Furthermore, all fibers infiltrated with water have flat dispersion characteristics. In particular, the dispersion of fibers #1, #3, and #4 fits into the NZD band in the full-infrared wavelength range. Fiber #3 has all normal dispersion in the anomalous NZD band. This fiber is therefore a good candidate for generation of a coherent supercontinuum.

Next, if we admit a change of temperature, even more flat dispersion can be obtained, as we see in the case of fibers #3 and #4. When temperature of these fibers infiltrated with water is increased to 80°C, a variation of dispersion characteristics is decreased to 0–27 ps/nm/km for fiber #3 and 0–35 ps/nm/km for fiber #4.

4. SIMULATIONS OF SUPERCONTINUUM GENERATION IN OPTIMIZED FIBERS

Based on the performed simulation, we have selected the fibers with optimum dispersion for supercontinuum generation simulations. The fiber SCF #3 infiltrated with water has a normal dispersion profile at room temperature with a flat plateau roughly between 900 and 1400 nm. Such so-called all-normal-dispersion fibers (ANDi fibers) have been shown to enable a coherent, pulse-preserving supercontinuum under femtosecond pumping [34].

The fiber labeled SCF #5, if made to operate at the slightly elevated temperature of 80°C, has an interesting dispersion profile with a positive slope, a ZDW at about 1000 nm, and a flat plateau of anomalous dispersion around 25 ps/nm/km extending from about 1200 nm. Both selected fibers can be efficiently pumped with ultrafast lasers operating at wavelengths close to 1 μm [34,35], which includes neodymium- or ytterbium-doped fiber lasers. In particular, fiber SCF #5 should enable an efficient supercontinuum light source when pumped with readily available stretched-pulse picosecond fiber lasers.

The ANDi SCF #3 requires femtosecond pumping if spectral broadening and excellent coherence and the temporal properties of the supercontinuum pulses are to be obtained. The modeling in each of the fibers has been performed using the standard generalized nonlinear Schrödinger equation (GNLSE), solved numerically using the split-step Fourier method—an implementation available in a textbook has been used [36]:

$$\frac{\partial A}{\partial z} + \frac{\alpha}{2}A - \sum_{k\geq 2}\frac{i^{k+1}}{k!}\beta_k\frac{\partial^k A}{\partial T^k} = i\gamma\left(1 + i\tau_{\text{shock}}\frac{\partial}{\partial T}\right) \times \left(A(z,t)\int_{-\infty}^{\infty} R(T')|A(z,T-T')|^2 \mathrm{d}T'\right). \quad (3)$$

The GNLSE in our modeling accounts for dispersion terms β_k up to the 9th order. The pump pulse assumed in the simulations was Gaussian-shaped, centered at 1064 nm.

A single photon per mode noise was added to the model. The fibers' mode effective areas were approximated with fixed values of their core areas, yielding 1.36 μm^2 and 7.54 μm^2 for SCF #3 and SCF #5, respectively. These values represent reasonable approximations compared to numerical data reported for water-filled suspended-core fibers provided in [8]. Measured Raman scattering spectra of the fiber glass were comparable to the silica glass; hence the Raman response identical to silica glass was used in both simulations, according to

$$R(T) = (1 - f_R)\cdot\delta(T) + f_R\frac{\tau_1^2+\tau_2^2}{\tau_1\tau_2^2}\exp(-T/\tau_2)\sin(T/\tau_1)\Theta(T), \quad (4)$$

where $f_R = 0.18$ is the delayed Raman contribution into the Kerr nonlinearity, $\tau_1 = 12.2$ fs, $\tau_2 = 32$ fs, $\Theta(t)$ is the Heaviside step function, and $\delta(t)$ is the Dirac delta function.

It is to be noted that in case of femtosecond ANDi supercontinuum generation, Raman processes are suppressed [34]. The nonlinear refractive index of the NC21A glass was measured using Z-scan at 1240 nm, $n_2 = 1.1\cdot 10^{-20}$ m^2/W [29]. We note that the nonlinearity of water was not included in the simulations. Water n_2 at 20°C is $1.9\cdot 10^{-20}$ m^2/W [37]. In our simulations, a simplifying assumption is made that the mode is mostly confined to the core, and it is the core glass nonlinearity which shapes the nonlinear response of the SCF in terms of n_2. The fiber loss was modeled using a 4 dB flat loss and the superposition of several Lorentzian lineshapes representing OH loss features in the vicinity of 1400 nm and 1800–1900 nm, peaking at +4 dB and +2 dB, respectively, above the flat loss background. A steep exponential edge

was used to model the glass transmission cut-off at about 2800 nm. The same loss characteristic was assumed in all simulations. The simulation results are shown in Figs. 10 and 11 for fibers SCF #3 and SCF #5, respectively, and the fiber loss spectrum applied in the simulations is shown in Fig. 12.

The pump source used in the SCF #3 simulation had a center wavelength of 1064 nm and 100 fs long Gaussian shaped pulses. Despite low nonlinearity (compared to, e.g., chalcogenide glass fibers or certain heavy metal oxide glass fibers reported in [26]) the fiber readily delivers an over-octave spanning, tabletop flat spectrum already at 2 nJ of pulse energy coupled into a 20 cm long fiber sample. In fact, the sample can be shortened several centimeters without any loss of spectral width, but the 20 cm was assumed for ease of handling in real experimental conditions. What is also notable is that there

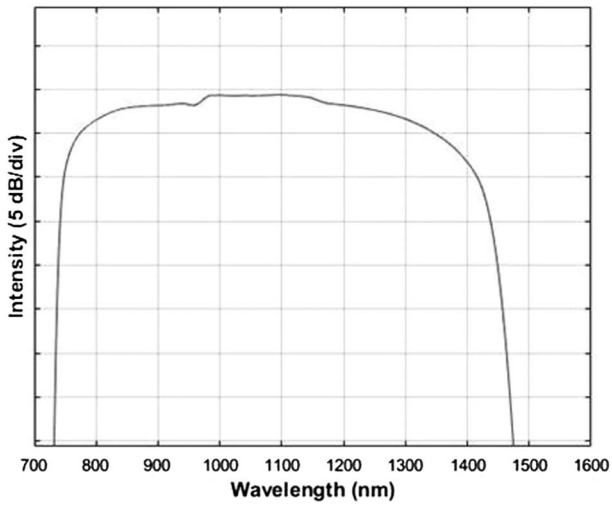

Fig. 10. Simulation of supercontinuum generation in the ANDi SCF #3 fiber infiltrated with water at room temperature, sample length 20 cm, 100 fs/1064 nm pump pulse, 2 nJ pulse energy.

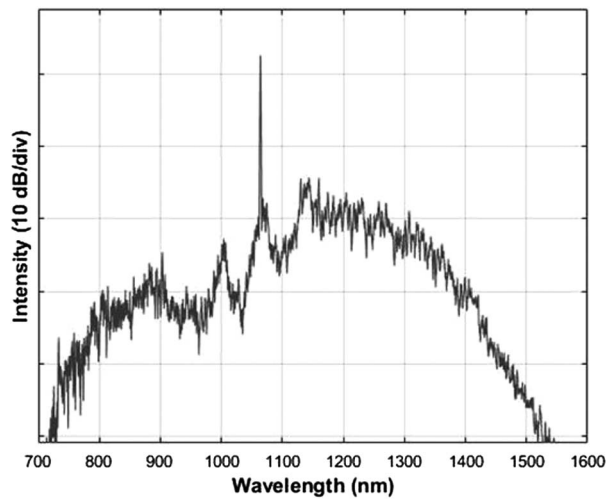

Fig. 11. Simulation of supercontinuum generation in the SCF #5 fiber assuming fiber temperature of 80°C and water infiltration of the air channels. Fiber length 1 m, pump parameters: 30 ps, 1064 nm, 10 nJ, Gaussian pulse shape.

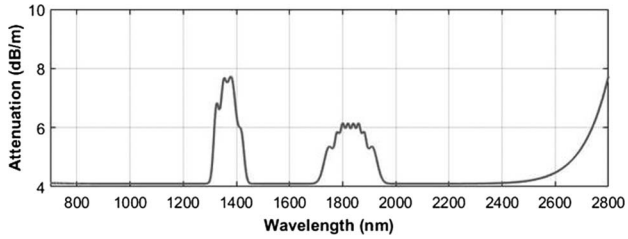

Fig. 12. Fiber attenuation spectrum used in numerical simulations.

seems to be practically no detrimental influence of fiber attenuation. This is explained for once with short propagation length and by the fact that the spectrum develops very quickly under femtosecond pumping. It is also notable that an ANDi octave-spanning supercontinuum is perfectly suited for application in few-cycle pulse generation, due to its high coherence and pulse shape quality [38]. We note that the difference in the effective areas of the two considered fibers is meaningful, because the SCF #3 fiber would be a factor of 5.5 more nonlinear than SCF #5 (roughly 500 1/W/km against 100 1/W/km). This is very convenient, because the normal dispersion of SCF #3 requires femtosecond pumping for practical spectral broadening. It can be expected that a robust femtosecond laser would come at a cost of limited pulse energy; then a high nonlinear coefficient would help to compensate for that. Simulation in the SCF #5 assumed a Gaussian pulse entered at 1064 nm and with a 30 ps duration. The spectrum shown in Fig. 10 was obtained under a reasonable 13 nJ of in-coupled energy in a 1 m long fiber sample. We note that a spectrum of comparable bandwidth in a lossless fiber scenario can be numerically obtained under 10 nJ pulses. The spectrum features significant structure despite 50 adjacent-points smoothing. This structure is related to the amplification of noise (modulation instability) being the main process contributing to spectral formation, which is expected at the assumed pump pulse durations [39]. Noise amplification is commonly known as an efficient means of generating broadband spectra, which would explain the limited influence of attenuation on bandwidth in the discussed scenario. Such a light source would have very poor coherence properties, but a spanning spectrum well over an octave is readily achieved under pumping from a relatively simple and robust laser.

5. CONCLUSIONS

We have shown that infiltration of air holes in suspended-core fibers with water significantly modifies the dispersion characteristics of suspended-core fibers made of borosilicate glass. The obtained dispersion is flat and reduced with respect to standard air hole SCFs. Variation of dispersion characteristics is usually below 50 ps/nm/km. This is very important since flat dispersion characteristics are required for efficient supercontinuum generation in fibers.

Furthermore, we observe that a zero dispersion wavelength is shifted toward longer wavelengths for over 200 nm into the proximity of 1000 nm. Shift of the ZDW toward 1000 nm is extremely important if we consider use of the SCF for supercontinuum generation with low-cost microchip lasers which

emit shot pulses. The modification of dispersion characteristics as well as matching the ZDW with the pump source wavelength of emission are in high demand for efficient supercontinuum generation.

Changing the temperature of the fiber infiltrated with water results in fine-tuning of the dispersion characteristics. As a result, the SCF with a core diameter of 1.64 μm has flat, all-normal dispersion if temperature is tuned to 80°C. This fiber can be used for coherent supercontinuum generation. The SCF with a core diameter of 2.66 μm has flat, near-zero anomalous dispersion in room temperature. This fiber can be used for soliton-based supercontinuum generation when pumped with picosecond shot pulses generated at 1064 nm by low-cost microchip lasers and would be suitable, e.g., for spectroscopy applications, in which an averaged signal response alleviating noise is sufficient.

The SCF infiltrated with water can be further modified if organic components and biomolecules are added. A water solution of bioluminescent particles used as a nonlinear medium was successfully used for enhancement of supercontinuum generation in the case of hollow-core PCFs [40]. On the other hand, further enhancement of thermal dispersion tuning can be achieved when water is replaced with other organic liquids with higher thermal expansion coefficients and lower absorption.

Funding. Narodowe Centrum Nauki (NCN) (DEC-2012/06/M/ST2/00479, UMO-2014/13/B/ST7/01742); Fundacja na rzecz Nauki Polskiej (FNP) (TEAM/2012-9/1).

Acknowledgment. The Foundation for Polish Science Team Programme is co-financed by the European Regional Development Fund, Operational Program Innovative Economy 2007–2013.

REFERENCES

1. P. Kaiser, E. A. J. Marcatili, and S. E. Miller, "A new optical fiber," Bell Syst. Tech. J. **52**, 265–269 (1973).
2. T. M. Monro, W. Belardi, K. Furusawa, J. C. Baggett, N. G. R. Broderick, and D. J. Richardson, "Sensing with microstructured optical fibers," Meas. Sci. Technol. **12**, 854–858 (2001).
3. A. S. Webb, F. Poletti, D. J. Richardson, and J. K. Sahu, "Suspended-core holey fiber for evanescent-field sensing," Opt. Eng. **46**, 010503 (2007).
4. M. Hautakorpi, M. Mattinen, and H. Ludvigsen, "Surface-plasmon-resonance sensor based on three-hole microstructured optical fiber," Opt. Express **16**, 8427–8432 (2008).
5. S. H. Aref, M. I. Zibaii, M. Kheiri, H. Porbeyram, H. Latifi, F. M. Araujo, L. A. Ferreira, J. L. Santos, J. Kobelke, K. Schuster, and O. Frazao, "Pressure and temperature characterization of two interferometric configurations based on suspended-core fibers," Opt. Commun. **285**, 269–273 (2012).
6. C. M. B. Cordeiro, C. J. S. de Matos, E. M. dos Santos, A. Bozolan, J. S. K. Ong, T. Facincani, G. Chesini, A. R. Vaz, and C. H. B. Cruz, "Towards practical liquid and gas sensing with photonic crystal fibers: side access to the fiber microstructure and single-mode liquid-core fiber," Meas. Sci. Technol. **18**, 3075–3081 (2007).
7. O. Frazao, R. M. Silva, M. S. Ferreira, J. L. Santos, and A. B. Lobo Ribeiro, "Suspended-core fibers for sensing applications," Photon. Sens. **2**, 118–126 (2012).
8. T. Monro, S. Warren-Smith, E. P. Schartner, A. François, S. Heng, H. Ebendorff-Heidepriem, and S. Afshar V., "Sensing with suspended-core optical fibers," Opt. Fiber Technol. **16**, 343–356 (2010).
9. F. Chu, G. Tsiminis, N. A. Spooner, and T. M. Monro, "Explosives detection by fluorescence quenching of conjugated polymers in suspended core optical fibers," Sens. Actuators B **199**, 22–26 (2014).
10. T. G. Euser, J. S. Y. Chen, M. Scharrer, P. St.J. Russell, N. J. Farrer, and P. J. Sadler, "Quantitative broadband chemical sensing in air-suspended solid-core fibers," J. Appl. Phys. **103**, 103108 (2008).
11. A. Mazhorova, A. Markov, A. Ng, R. Chinnappan, O. Skorobogata, M. Zourob, and M. Skorobogatiy, "Label-free bacteria detection using evanescent mode of a suspended core terahertz fiber," Opt. Express **20**, 5344–5355 (2012).
12. K. Kosma, G. Zito, K. Schuster, and S. Pissadakis, "Whispering gallery mode microsphere resonator integrated inside a microstructured optical fiber," Opt. Lett. **38**, 1301–1303 (2013).
13. S. Afshar V., W. Q. Zhang, H. Ebendorff-Heidepriem, and T. M. Monro, "Small core optical waveguides are more nonlinear than expected: experimental confirmation," Opt. Lett. **34**, 3577–3579 (2009).
14. T. Cheng, R. Usaki, Z. Duan, W. Gao, D. Deng, M. Liao, Y. Kanou, M. Matsumoto, T. Misumi, T. Suzuki, and Y. Ohishi, "Soliton self-frequency shift and third-harmonic generation in a four-hole As_2S_5 microstructured optical fiber," Opt. Express **22**, 3740–3746 (2014).
15. M. Duhant, W. Renard, G. Canat, T. N. Nguyen, F. Smektala, J. Troles, Q. Coulombier, P. Toupin, L. Brilland, P. Bourdon, and G. Renversez, "Fourth-order cascaded Raman shift in AsSe chalcogenide suspended-core fiber pumped at 2 μm," Opt. Lett. **36**, 2859–2861 (2011).
16. W. Gao, M. El Amraoui, M. Liao, H. Kawashima, Z. Duan, D. Deng, T. Cheng, T. Suzuki, Y. Messaddeq, and Y. Ohishi, "Mid-infrared supercontinuum generation in a suspended-core As_2S_3 chalcogenide microstructured optical fiber," Opt. Express **21**, 9573–9583 (2013).
17. I. Savelli, O. Mouawad, J. Fatome, B. Kibler, F. Désévédavy, G. Gadret, J.-C. Jules, P.-Y. Bony, H. Kawashima, W. Gao, T. Kohoutek, T. Suzuki, Y. Ohishi, and F. Smektala, "Mid-infrared 2000-nm bandwidth supercontinuum generation in suspended-core microstructured Sulfide and Tellurite optical fibers," Opt. Express **20**, 27083–27093 (2012).
18. C. Chaudhari, T. Suzuki, and Y. Ohishi, "Design of zero chromatic dispersion chalcogenide As_2S_3 glass nanofibers," J. Lightwave Technol. **27**, 2095–2099 (2009).
19. M. Szpulak and S. Fevrier, "Chalcogenide As_2S_3 suspended core fiber for mid-IR wavelength conversion based on degenerate four-wave mixing," IEEE Photon. Technol. Lett. **21**, 884–886 (2009).
20. M. El-Amraoui, J. Fatome, J. C. Jules, B. Kibler, G. Gadret, C. Fortier, F. Smektala, I. Skripatchev, C. F. Polacchini, Y. Messaddeq, J. Troles, L. Brilland, M. Szpulak, and G. Renversez, "Strong infrared spectral broadening in low-loss As-S chalcogenide suspended core microstructured optical fibers," Opt. Express **18**, 4547–4556 (2010).
21. E. Coscelli, F. Poli, J. Li, A. Cutinotte, and S. Selleri, "Dispersion engineering of highly nonlinear chalcogenide suspended-core fiber," IEEE Photon. J. **7**, 1–8 (2015).
22. A. Bozolan, C. J. S. de Matos, C. M. B. Cordeiro, E. M. dos Santos, and J. Travers, "Supercontinuum generation in a water-core photonic crystal fiber," Opt. Express **16**, 9671–9676 (2008).
23. J. Bethge, A. Husakou, F. Mitschke, F. Noack, U. Griebner, G. Steinmeyer, and J. Herrmann, "Two-octave supercontinuum generation in a water-filled photonic crystal fiber," Opt. Express **18**, 6230–6240 (2010).
24. N. Karasawa, "Dispersion properties of liquid-core photonic crystal fibers," Appl. Opt. **51**, 5259–5265 (2012).
25. E. Yoshida, A. Wada, and N. Karasawa, "Supercontinuum generation using a selectively water-filled photonic crystal fiber for enhancement in the visible spectral region," Jpn. J. Appl. Phys. **55**, 072501 (2016).
26. R. Stępień, J. Cimek, D. Pysz, I. Kujawa, M. Klimczak, and R. Buczyński, "Soft glasses for photonic crystal fibers and microstructured optical components," Opt. Eng. **53**, 071815 (2014).
27. I. Kujawa, R. Buczynski, T. Martynkien, M. Sadowski, D. Pysz, R. Stepien, A. J. Waddie, and M. R. Taghizadeh, "Multiple defect core photonic crystal fiber with high birefringence induced by squeezed lattice with elliptical holes in soft glass," Opt. Fiber Technol. **18**, 220–225 (2012).

28. R. Buczynski, D. Pysz, R. Stepien, A. J. Waddie, I. Kujawa, R. Kasztelanic, M. Franczyk, and M. R. Taghizadeh, "Supercontinuum generation in photonic crystal fibers with nanoporous core made of soft glass," Laser Phys. Lett. **8**, 443–448 (2011).
29. D. Lorenc, I. Bugar, M. Aranyosiova, R. Buczynski, D. Pysz, D. Velic, and D. Chorvat, "Linear and nonlinear properties of multicomponent glass photonic crystal fibers," Laser Phys. **18**, 270–276 (2008).
30. A. V. Mitrofanov, Y. M. Linik, R. Buczynski, D. Pysz, D. Lorenc, I. Bugar, A. A. Ivanov, M. V. Alfimov, A. B. Fedotov, and A. M. Zheltikov, "Highly birefringent silicate glass photonic-crystal fiber with polarization-controlled frequency-shifted output: a promising fiber light source for nonlinear Raman microspectroscopy," Opt. Express **14**, 10645–10651 (2006).
31. Lumerical Eigenmode Expansion (EME) Solver, https://www.lumerical.com/tcad-products/mode/EME, accessed 29 August 2016.
32. T. Martynkien, D. Pysz, R. Stępień, and R. Buczyński, "All-solid microstructured fiber with flat normal chromatic dispersion," Opt. Lett. **39**, 2342–2345 (2014).
33. I. Thomrmahlen, J. Straub, and U. Grigull, "Refractive index of water and its dependence on wavelength, temperature and density," J. Phys. Chem. Ref. Data **14**, 933–945 (1985).
34. A. M. Heidt, A. Hartung, G. W. Bosman, P. Krok, E. G. Rohwer, H. Schwoerer, and H. Bartelt, "Coherent octave spanning near-infrared and visible supercontinuum generation in all-normal dispersion photonic crystal fibers," Opt. Express **19**, 3775–3787 (2011).
35. J. M. Dudley, G. Genty, and S. Coen, "Supercontinuum generation in photonic crystal fiber," Rev. Mod. Phys. **78**, 1135–1184 (2006).
36. J. C. Travers, M. H. Frosz, and J. M. Dudley, "Nonlinear fiber optics overview," in *Supercontinuum Generation in Optical Fibers*, J. M. Dudley and R. Taylor, eds. (Cambridge University, 2010), pp. 32–51.
37. Z. W. Wilkes, S. Varma, Y.-H. Chen, H. M. Milchberg, T. G. Jones, and A. Ting, "Direct measurements of the nonlinear index of refraction of water at 815 and 407 nm using single-shot supercontinuum spectral interferometry," Appl. Phys. Lett. **94**, 211102 (2009).
38. A. M. Heidt, J. Rothhardt, A. Hartung, H. Bartelt, E. G. Rohwer, J. Limpert, and A. Tünnermann, "High quality sub-two cycle pulses from compression of supercontinuum generated in all-normal dispersion photonic crystal fiber," Opt. Express **19**, 13873–13879 (2011).
39. J. M. Dudley and S. Coen, "Coherence properties of supercontinuum spectra generated in photonic crystal and tapered optical fibers," Opt. Lett. **27**, 1180–1182 (2002).
40. Y. Cho, B. Park, J. Oh, M. Seo, K. Lee, C. Kim, T. Lee, D. H. Woo, S. Lee, H. M. Kim, H. Lee, K. Oh, D. Yeom, S. R. Dugasani, S. H. Park, and J. H. Kim, "Broadband supercontinuum generation using a hollow optical fiber filled with copper-ion-modified DNA," Opt. Express **23**, 13537–13544 (2015).